Two-dimensional direct numerical simulation of spray flames. Part 2: Effects of ambient pressure and lift, and validity of flamelet model

Tomoaki Kitano, Tomoaki Nakatani, Ryoichi Kurose*, Satoru Komori

Department of Mechanical Engineering and Science, and Advanced Research Institute of Fluid Science and Engineering, Kyoto University, Yoshida-honmachi, Sakyo-ku, Kyoto, Kyoto 606-8501, Japan

Abstract

The effect of ambient pressure on spray flames is investigated by means of two-dimensional direct numerical simulation (DNS), and the validity of an extended flamelet /progress-variable approach (EFPV) is examined under the high-pressure condition. The DNS is performed not only for a simple jet spray flame with a pilot burner but also for a lifted recirculation spray flame without any pilot burner at ambient pressures of 0.1 and 0.5 MPa. *n*-decane ($C_{10}H_{22}$) is used as liquid spray fuel, and the evaporating droplets' motions are tracked by the Lagrangian method. The results show that the behaviors of jet and lifted recirculation spray flames are strongly affected by ambient pressure. The effects of the change of the ambient pressure on these spray flame behaviors can be well captured by EFPV and EFPV coupled with *G*-equation model (EFPV-G), respectively.

Keywords: Numerical simulation; Spray combustion; Jet flame; High pressure; Lifted flame; Flamelet model

*Corresponding author. fax: +81 75 753 9218.
Email address: kurose@mech.kyoto-u.ac.jp (Ryoichi Kurose)

1. Introduction

The effects of ambient pressure on the spray combustion behavior have not been well clarified yet mainly because combustion conditions and acquired properties are extremely limited due to the difficulty of the measurements [e.g., 1-4]. Recent progresses of direct numerical simulation (DNS) and large-eddy simulation (LES) of spray combustion fields [e.g., 5-17] enable us to numerically investigate the effects of the ambient pressure on the spray combustion behavior in detail. However, these simulations are still very expensive so that the spray combustion mechanism has not been examined enough yet. One of the important research subjects is how premixed and diffusion flames contribute in the spray flames, which could be an indication for the combustion modeling. Nakamura et al. [5] and Baba and Kurose [10] investigated the contributions of the premixed and diffusion flames in spray flames in a counterflow and a jet, respectively, by means of two-dimensional DNS, and Luo et al. [13] extended the discussion by means of three-dimensional DNS. Moreover, Baba and Kurose [10] examined the applicability of flamelet models [e.g., 18-20], which are originally proposed for gaseous combustion, to the combustion model of jet spray flames by means of two-dimensional DNS, and found that the flamelet/progress-variable approach (referred to as FPV, in this study) [20] is valid in general. However, the contributions of the premixed and diffusion flames and the applicability of FPV were mainly studied under the atmospheric pressure condition of 0.1 MPa and the effects of the ambient pressure have not been investigated enough. In addition, the flames considered in these studies by two-dimensional DNS were simple jet flames with a pilot burner because of the difficulty in maintaining the two-dimensional stable spray flames without forced ignition, but the flames observed in actual engines are swirling-recirculation flames without any pilot burner. Therefore, the study on more realistic flames is essential.

The purpose of this study is to investigate the effects of various combustion conditions on the spray combustion behavior by means of two-dimensional DNS of spray jet flames. The present paper provides the second part of two investigations. In part 1 [21], the effects of equivalence ratio, fuel droplet size and radiation on the spray combustion behavior were investigated. In addition, the validity of the extended

flamelet/progress-variable approach (referred to as EFPV, in this paper) was examined in various equivalence-ratio and fuel-droplet-size conditions and in the presence of the radiation. In this part 2, the effect of ambient pressure on the spray combustion behavior and the validity of EFPV in high-pressure condition are studied. The two-dimensional DNS is applied to spray flames at ambient pressures of 0.1 and 0.5 MPa and the validity of EFPV is examined by comparing with the results using the direct combustion model based on the Arrhenius formation (referred to as ARF, in this paper). The flames considered are not only a simple jet spray flame with a pilot burner but also a lifted recirculation spray flame without any pilot burner which has been established for investigating the more realistic flames. n-decane ($C_{10}H_{22}$) is used as liquid spray fuel, and the evaporating droplets' motions are tracked by the Lagrangian method.

2. Numerical Simulation

2.1. Numerical methods for ARF, EFPV and EFPV-G

The set of governing equations of the carrier gaseous phase and dispersed droplets phase for ARF and EFPV are described in our previous papers [5, 8, 9, 10, 12] and part 1 [21] of this study. The combustion reaction of the evaporated n-decane with oxygen is described using a one-step global reaction model [22] as $C_{10}H_{22} + \frac{31}{2}O_2 \rightarrow 10CO_2 + 11H_2O$.

In order to take into account the effect of high ambient pressure, boiling temperature, T_{BL}, and latent heat of droplet evaporation, L_V, of liquid droplet at ambient pressure of P are given by

$$\begin{aligned} T_{BL} &= \left(\frac{P^{0.119}+c}{11.9}\right)^{-0.119}, \\ c &= P_{atm} - 11.9T_{BL,atm}^{0.119}, \end{aligned} \tag{1}$$

$$L_V = L_{V,T_{BL,atm}} \left(\frac{T_{CL}-T_d}{T_{CL}-T_{BL,atm}}\right)^{0.38}, \tag{2}$$

respectively. Here, the subscript atm means the value under atmospheric pressure. $L_{V,T_{BL}}$, T_{BL} and T_{CL} are the latent heat of droplet evaporation, the boiling temperature

and the critical temperature, respectively [5]. T_d is the droplet temperature. All thermophysical properties values and transport coefficients under various pressures are obtained from CHEMKIN [23,24]. Radiation effect [9, 21] is neglected in this study.

It is known that the flame which lifts off from the nozzle or burner and stabilize at a suspended region is called "lifted flame" and that in the lifted flame, the remixed flame forms upstream of the diffusion flame and plays an important role to stabilize the lifted flame (this flame is called "partially premixed flame"). This fact suggests that EFPV based on the diffusion flame cannot be simply applied to the lifted flame. Concerning the premixed combustion, an equation describing the dynamics of a laminar flame front, known as G-equation, has been presented by Williams [25]. Accordingly, Muller et al. [26] proposed a method for the partially premixed flame, in which the premix and diffusion flame models are combined. Based on their concept coupled with FPV, in addition to the equations of Z and C, the G-equation should be solved simultaneously. The scalar G is used to distinguish between the combusting and non-combusting regions (i.e., $G > 0$ and $G < 0$ show the combusting and non-combusting regions, respectively), and the scalars Z and C are used to characterize the combusting region. Recently, the concept of Muller et al. [26] for the gaseous combustion was examined for the spray combustion by Baba and Kurose [27]. For the lifted recirculation spray flame, therefore, EFPV coupled with the G-equation based on [31] is also tested. The laminar burning velocity s_L in the G-equation is modeled as a function of Z, i.e., $s_L = s_L(Z)$ by solving a one-dimensional governing equations for gaseous premixed flame. It was observed that as the ambient pressure increases s_L decreases. This trend agrees with previous study [e.g., 32]. This numerical method is referred to as EFPV-G, hereafter.

2.2. Computational details

The computational details adopted here are basically the same as our previous study [10,21]. Fig. 1 shows the schematic of computational domains and inlet conditions for a simple jet spray flame with a pilot burner and a lifted recirculation spray flame without any pilot burner. The length and velocity are non-dimensionalized by the reference length ($L_0 = 1.5 \times 10^{-2}$ m) and velocity ($U_0 = 15$ m s^{-1}), respectively. For the jet spray flame, the dimensions of the computational domain are 5 and 2 in

the streamwise and spanwise directions ($0 \leq x \leq 5$ and $-1 \leq y \leq 1$), respectively. The stoichiometric mixture gas is issued from the inlets of $0.060 < y < 0.075$ and $-0.075 < y < -0.060$ as coflows to stably ignite the flame, and air is issued from the other inlets. The stoichiometric mixture properties are obtained from the flamelet library. The inflow velocities of the air carring fuel droplets, coflow and outer air are set to be U= 1, 1, 0.2, respectively. The velocity perturbations based on continuous sine functions with a magnitude of 5 % are imposed in the inflow velocities of the air carring fuel droplets (see part 1 [21]). The inflow gas temperature non-dimensionalized by reference temperature (T_0 = 300 K) is set to be $T = 1$, except the inlets for the stoichiometric mixture gas. Reynolds number, Re, based on the jet width and velocity is 2250. The fuel droplets (spray) with a certain size distribution are injected from the central inlet of $-0.065 < y < 0.065$ with air. The equivalence ratio, ϕ, based on the air flow rate issued at the center port is 10, and the the averaged non-dimensional initial droplet diameter is set to be 3.33×10^{-3} with the minimum and maximum values of 6.7×10^{-5} and 6.7×10^{-3}, respectively. Initial droplet locations are randomly given at x = 0, and the velocities are set to be equivalent to the gas-phase velocities at the center of the droplets. The computational domain is divided into 1000 (in the x direction) $\times$ 440 (in the y direction) non-uniform computational grid points, and fine resolution is given around the center of the stream lines.

For the lifted recirculation spray flame, the dimensions of the computational domain are 4 and 2 in the streamwise and spanwise directions ($0 \leq x \leq 4$ and $-1 \leq y \leq 1$), respectively. The inflow velocities of the center flow ($-0.13 < y < 0.13$), air carring fuel droplets ($0.13 < y < 0.20$ and $-0.20 < y < -0.13$) and outer air flows ($0.20 < y < 0.67$, $-0.67 < y < -0.20$, $0.67 < y < 1.0$ and $-1.0 < y < -0.67$) are set to be U= 0.067, 0.067, 1.4, 0.067 respectively. The inflow gas temperature non-dimensionalized by reference temperature (T_0 = 300 K) is set to be $T = 1$. Reynolds number, Re, based on the the spray jet width and the slip velocity between the spray jet and the outer flow (i.e., $1.3U_0$) is 1250. The equivalence ratio, ϕ, based on the air flow rate issued at the center port is 12, and the the averaged non-dimensional initial droplet diameter is set to be 1.0×10^{-3} with the minimum and maximum values

of 6.7×10^{-5} and 2.0×10^{-3}, respectively, using a homogeneous droplet diameter distribution. Initial droplet locations are randomly given at $x = 0$, and the velocities are set to be equivalent to the gas-phase velocities at the center of the droplets. The computational domain is divided into 400 (in the x direction) $\times$ 300 (in the y direction) non-uniform computational grid points, and fine resolution is given around the center of the stream lines.

The boiling temperature of droplet under atmospheric pressure is $T_{BL,atm}$ =447.7 K, the heat capacity is c_L = 2520.5 J kg^{-1} K^{-1} and the density is ρ = 642 kg m^{-3}. The latent heat of droplet at boiling temperature under atmospheric pressure is $L_{V,T_{BL,atm}}$ =279.4 kJ kg^{-1}. The governing equations of the carrier gas phase are discretized on a staggard mesh arrangement to construct fully conservative finite-difference formulations. The spatial derivatives in these equations are approximated by a second-order accurate central difference scheme. Only for the convection terms of the conservation equations of energy and mass fractions of chemical species, the QUICK scheme is employed. For the discretization of the G-equation, the advection term is approximated by the third-order accurate ENO scheme. A convective outflow condition is applied to the outflow boundary of the streamwise direction. The slip wall condition is applied to the spanwise direction. The fractional step method and the second-order explicit Runge-Kutta method are used for the time advancement of the carrier gas and dispersed droplet phases, respectively.

Table 1 lists the cases performed in this study. For both the jet spray flame and the lifted recirculation spray flame, the detailed spray flame behavior is investigated by ARF, and the ARF results are used as references to validate EFPV and EFPV-G. The CPU time for the computations in the cases of 0.5 MPa are about 1.3 times larger than those in the cases of 0.1 MPa. The CPU times for J-2 and L-2 in Table 1 in which 42,000 and 500,000 droplets are tracked respectively are about 63 h and 115 h for 50,000 steps on NEC: SX-8, respectively.

3. Results and discussion

3.1. Jet spray flame behavior predicted by ARF

Fig. 2 shows the distributions of instantaneous gas temperature, T, for J-1 – J-4. It is clearly observed that the high-temperature region on the edge of the flame have thinner and more-disturbed configurations for J-2 than for J-1 and that extinctions appear at some locations for J-2. These are due to the facts that as the ambient pressure increases, turbulence becomes strong due to the increase in density (i.e., Reynolds number) and flame thickness becomes thin due to the increase in reaction rate. The behavior for J-3 and J-4 by EFPV will be discussed later.

The comparisons of the scatter plot of instantaneous gas temperature, T, against mixture fractions, Z, and the comparison of the spanwise profile of time-averaged gas temperature, $\overline{T}$, at four streamwise locations between J-1 and J-2 are shown in Fig. 3. The values of the instantaneous gas temperature for J-2 are generally higher than those for J-1 at a fixed Z, whereas the peaks of the time-averaged gas temperature for J-2 are lower than those for J-1 at all streamwise locations and the discrepancy becomes marked downstream. This was due to the fact that compared to J-1 the turbulence intensities for J-2 markedly increased downstream, which acted to diffuse the heat of the high-temperature region to outer regions.

Fig. 4 shows the comparison of the distribution of instantaneous flame index, FI, between J-1 and J-2. Here, FI is a parameter used for discriminating premixed flame and diffusion flame [28], and given by $FI = \nabla Y_{\mathrm{C_{10}H_{22}}} \cdot \nabla Y_{\mathrm{O_2}}$. The positive and negative FI mean the premixed flame and diffusion flame, respectively. As reported by Baba and Kurose [10] and Fujita et al. [21], the spray flame consists of the diffusion and premixed flames. Also the diffusion flames exist both in the central and edge regions of the jet, whereas the premixed flames appear mainly in the central region. Furthermore, it is found that the premixed flames tend to exist along with the diffusion flames and that the premixed flames for J-2 are weaker than that for J-1 in the upstream region.

In order to clarify the mechanism, the spanwise profiles of the time-averaged reaction rate, $\overline{\dot{m}}_F$, and mass fractions of fuel gas ($\mathrm{C_{10}H_{22}}$) and oxygen, $\overline{Y}_F$ and $\overline{Y}_O$, at $x = 0.2$ where the difference between J-1 and J-2 is marked are compared in Fig. 5. Here,

the zones where the premixed and diffusion flames appear are indicated by "pre" and "$diff$" in the figure, respectively. According to the definition, the premixed flames exist in the zones where both fuel and oxygen increase or decrease at the same time, and the diffusion flames exist in the zones where fuel and oxygen indicate different trend with respect to the y direction. It is found that the premixed flame does not occur during the fuel increasing with increasing y due to high evaporation rate, but it begins to appear once fuel turns to decrease after its peak, because oxygen still continuously decreases with increasing y in this zone. Thus, the premixed flames tend to exist along with the diffusion flame, where the fuel consumption rate due to reaction is higher than the fuel production rate due to evaporation and oxygen still remains. Hence, in the condition where the oxygen consumption rate is much higher due to high reaction rate such as for J-2, the zero-oxygen zone clearly appears, which makes the premixed flame zone thinner.

3.2. Lifted recirculation spray flame behavior predicted by ARF

Fig. 6 shows the distributions of instantaneous gas temperature, T, for L-1 – L-6, and Fig. 7 shows the comparison of the spanwise profiles of time-averaged gas temperature, $\overline{T}$, at two streamwise locations between L-1 and L-2. It is observed that for both cases of L-1 and L-2 the stable lifted flame without any forced ignition is achieved. However, these flames tended to gradually weaken with time so that above and below statistics are taken during the periods that the appearances of these flames don't change very much. The instantaneous gas temperature on the flame edges is higher for L-2 than for L-1, whose trend is similar to that for the jet spray flame. However, unlike the jet spray flame, the time-averaged gas temperature for L-2 tends to be higher than that for L-1. This is was due to the fact that the vortices generated for L-2 were stronger than those for L-1, which enhanced the entrainment of fuel droplets into the central region, the enlargement of their residence time, the droplet evaporation, and consequently the combustion reaction. The generations of the strong vortices are considered to be generated by the stronger fluid shear at the high ambient pressure. due to the fact that the higher the ambient pressure is, the narrower the reaction zone is, which creates the stronger fluid shear. The behavior for L-3 – L-6 by EFPV and

EFPV-G will be discussed later.

Fig. 8 shows the comparison of the distribution of instantaneous flame index, FI, between L-1 and L-2. Similarly to the jet spray flame, the premixed flames tend to exit along with the diffusion flames and that the premixed flames for L-2 are weaker than that for L-1. The spanwise profiles of the time-averaged reaction rate, $\overline{\dot{m}}_F$, and mass fractions of fuel gas ($C_{10}H_{22}$) and oxygen, $\overline{Y}_F$ and $\overline{Y}_O$, at $x = 1.3$ where the difference between L-1 and L-2 is marked are compared in Fig. 9. Although the supply condition of oxygen is different from the jet spray flame (i.e., the oxygen is supplied both from outer and inner streams for the jet spray flame, whereas it is supplied only from outer stream for the lifted recirculation spray flame in this region), the reason why the premixed flame becomes weak in the high-pressure condition is similarly explained. That is, in the condition where the oxygen consumption rate is much higher than the production rate due to high reaction rate in the high-pressure condition, the zero-oxygen zone widely appears in the flame and this makes the premixed flame zone thinner.

3.3. Applicability of EFPV and EFPV-G

Fig. 10 shows the comparision of the spanwise profiles of time-averaged gas temperature, $\overline{T}$, obtained by EFPV (J-3 and J-4), together with the profiles obtained by ARF (J-1 and J-2). This comparison and Fig. 2 show that EFPV can properly capture the effect of the ambient pressure. That is, as the ambient pressure increases, the instantaneous gas temperature on the edge of the flame increases and the high-temperature region becomes thin, whereas the time-averaged temperature decreases. However, the quantitative discrepancies in the time-averaged value are observed in the central region between J-1 and J-3, and J-2 and J-4. The reason of these discrepancies was explaind in part 1 [21] related to the facts that the mixture fraction, Z, for the spray combustion is not the conserved scalar and the flamelet model is basically weak at capturing the ignition and premixed flame. In fact, it is apparent that as the ambient pressure increases, namely as the premixed flame decreases in the upstream region, the discrepancy in the gas temperature in the central region becomes small between ARF and EFPV.

As shown in Fig. 6, the comparison with the predictions by ARF verifies that the employment of the G-equation model drastically improves the performance, namely the lifted flame is achieved only for EFPV-G. Fig. 11 shows the comparison of the spanwise profile of time-averaged gas temperature, $\overline{T}$, for the lifted recirculation spray flame among ARF (L-1 and L-2), EFPV (L-3 and L-4) and EFPV-G (L-5 and L-6). Regardless of the ambient pressure, the EFPV-G is found to be superior to EFPV especially in the upstream region. Thus, the coupling of the G-equation model with the extended flamelet/progress-variable approach is obviously valid for the lifted recirculation spray flame. Compared to the jet spray flame described above, the discrepancy between ARF and EFPV is not evident very much even in the condition of ambient pressure of 0.1 MPa. This is considered due to that for the lifted recirculation spray flame, the flame behavior in the upstream region hardly affects that in the downstream region owing to the presence of strong recirculation.

4. Conclusions

The effect of ambient pressure on jet spray flames was investigated by means of two-dimensional direct numerical simulation (DNS), and the validity of an extended flamelet/progress-variable approach (EFPV) was examined under the high-pressure condition. The DNS was performed not only for a simple jet spray flame with a pilot burner but also for a lifted recirculation spray flame without any pilot burner at ambient pressures of 0.1 and 0.5 MPa. n-decane ($C_{10}H_{22}$) was used as liquid spray fuel, and the evaporating droplets' motions were tracked by the Lagrangian method. The main results obtained in this study can be sumrized as follows.

(1) For both the jet and lifted recirculation spray flames, the high-temperature region on the edge of the flame becomes thinner and the contribution of premixed flame decreases, as the ambient pressure increases.

(2) The effect of the change of the ambient pressure on these spray flame behaviors can be well captured by EFPV and EFPV-G.

Acknowledges

The authors are grateful to Dr. Hiroaki Watanabe of Central Research Institute of Electric Power Industry (CRIEPI), Dr. Mariko Nakamura of Osaka University, and Dr. Akitoshi Fujita, and Mr. Yutaka Yano of Kyoto University for many useful discussions. A portion of this research was supported by the grant for "Strategic Program - Research Field No. 4: Industrial Innovations" from the Ministry of Education, Culture, Sports, Science, and Technology (MEXT)'s "Development and Use of Advanced, High-Performance, General-Purpose Supercomputers Project".

References

[1] Cooper CS, Laurendeau NM. Quantitative measurements of nitric oxide in high-pressure (2-5 atm), swirl-stabilized spray flames via laser-induced fluorescence. Combust Flame 2000;123:175-188.

[2] Russo S, Gomez A. Physical characterization of laminar spray flames in the pressure range 0.1-0.9 MPa. Combust Flame 2006;145:339-356.

[3] Ryser R, Gerber T, Dreier T. Soot particle sizing during high-pressure Diesel spray combustion via time-resolved laser-induced incandescence. Combust Flame 2009;156:120-129.

[4] Nakamura M, Nishioka D, Hayashi J, Akamatsu F. Soot particle sizing during high-pressure Diesel spray combustion via time-resolved laser-induced incandescence. Combust Flame 2011;158:1615-1623.

[5] Nakamura M, Akamatsu F, Kurose R, Katsuki M. Combustion mechanism of liquid fuel spray in a gaseous flame. Phys Fluids 2005;17:123301.

[6] Domingo P, Vervisch L, Réveillon J. DNS analysis of partially premixed combustion in spray and gaseous turbulent flame-bases stabilized in hot air. Combust Flame 2005;140:172-195.

[7] Réveillon J, Vervisch L. Analysis of weakly turbulent dilute-spray flames and spray combustion regimes. J Fluid Mech 2005;537:317-347.

[8] Watanabe H, Kurose R, Hwang H.-S, Akamatsu F. Characteristics of flamelets in spray flames formed in a laminar counterflow. Combust Flame 2007;148:234-248.

[9] Watanabe H, Kurose R, Komori S, Pitsch H. Effects of radiation on spray flame characteristics and soot formation. Combust Flame 2008;152:2-13.

[10] Baba Y, Kurose R. Analysis and flamelet modelling for spray combustion. J Fluid Mech 2008;612:45-79.

[11] Neophytou A, Mastorakos E, Cant RS. DNS of spark ignition and edge flame propagation in turbulent droplet-laden mixing layers. Combust Flame 2010;157:1071-1086.

[12] Hayashi J, Watanabe H, Kurose R, Akamatsu F. Effects of fuel droplet size on soot formation in spray flames formed in a laminar counterflow. Combust Flame 2011;158:2559-2568.

[13] Luo K, Pitsch H, Pai MG, Desjardins O. Direct numerical simulations and analysis of three-dimensional n-heptane spray flames in a model swirl combustor. Proc Combust Inst 2011;33:2143-2152.

[14] Moin P, Apte SV. Large-eddy simulation of turbulent combustion. AIAA J 2006;44:698-708.

[15] Boileau M, Pascaud S, Riber E, Cuenot B, Gicquel LYM, Poinsot TJ. Investigation of Two-Fluid Methods for Large Eddy Simulation of Spray Combustion in Gas Turbines. Turb Combust 2008;80:291-321.

[16] Patel N, Menon S. Simulation of spray-turbulence-flame interactions in a lean direct injection combustor. Combust Flame 2008;153:228-257.

[17] Ihme M, Pitsch H. Modeling of radiation and nitric oxide formation in turbulent nonpremixed flames using a flamelet/progress variable formulation. Phys Fluids 2008;20:055110.

[18] N. Peters. Turbulent combustion Cambridge University Press Cambridge 2000.

[19] Pitsch H, Steiner H. Large-eddy simulation of premixed turbulent combustion using a level-set approach. Phys Fluids 2000;12:2541-2554.

[20] Pierce CP, Moin P. Progress-variable approach for large-eddy simulation of non-premixed turbulent combustion. J Fluid Mech 2004;504:73-97.

[21] Fujita A, Watanabe H, Kurose R, Komori S. Two-dimensional direct numerical simulation of spray flames. Part 1: Effects of equivalence ratio, fuel droplet size and radiation, and validity of flamelet model. Fuel submitted.

[22] Westbrook CK, Dryer FL. Chemical kinetic modeling of hydrocarbon combustion. Prog Energy Combust Sci 1984;10:1-57.

[23] Kee RJ, Dixon-Lewis G, Warnatz J, Coltrin ME, Miller JA. A fortran computer code package for evaluation of gas-phase multi-component transport properties. Sandia Report 1984;SAND86-8246.

[24] Kee RJ, Rupley FM, Miller JA. CHEMKIN-II: A FORTRAN chemical kinetics package for the analysis of gas phase chemical kinetics. Sandia Report 1989;SAND89-8009B.

[25] F.A. Williams The Mathematics of Combustion (ed. J. Buckmaster) SIAM 1985;99-131.

[26] Muller CM, Breitbach H, Peters N. Partially premixed turbulent flame propagation in jet flames. Proc Combust Inst 1994;25:1099-1106.

[27] Baba Y, Kurose R. Flamelet Characteristics of Gaseous and Spray Lifted Flames on Two-Dimensional Direct Numerical Simulation. J Fluid Sci Technol 2008;3:846-856.

[28] Yamashita H, Shimada M, Takeno T. A numerical study on flame stability at the transition point of jet diffusion flames. Proc Combust Inst 1996;26:27-34.

NOMENCLATURE

C	progress variable, -
c_L	specific heat of liquid fuel, J kg^{-1} K^{-1}
c_p	specific heat of mixture gas, J kg^{-1} K^{-1}
FI	flame index, -
L	length, m
L_V	latent heat of droplet evaporation, J kg^{-1}
P	gaseous pressure, Pa
s_L	laminar burning velocity, m/s
T	gaseous temperature, K
U	velocity, s^{-1}
Y_k	mass fraction of kth species, -
Z	mixture fraction, -
ϕ	equivalence ratio, -
ρ	density, kg m^{-3}
atm	atmospheric
BL	boiling point
CL	critical point
F	fuel gas
O	oxidizer
0	reference value

LIST OF TABLE AND FIGURE

Table 1:

	Case	Model	Ambient pressure [MPa]
Jet spray flame	J-1	AFR	0.1
	J-2	AFR	0.5
	J-3	EFPV	0.1
	J-4	EFPV	0.5
Lifted recirculation spray flame	L-1	AFR	0.1
	L-2	AFR	0.5
	L-3	EFPV	0.1
	L-4	EFPV	0.5
	L-5	EFPV-G	0.1
	L-6	EFPV-G	0.5

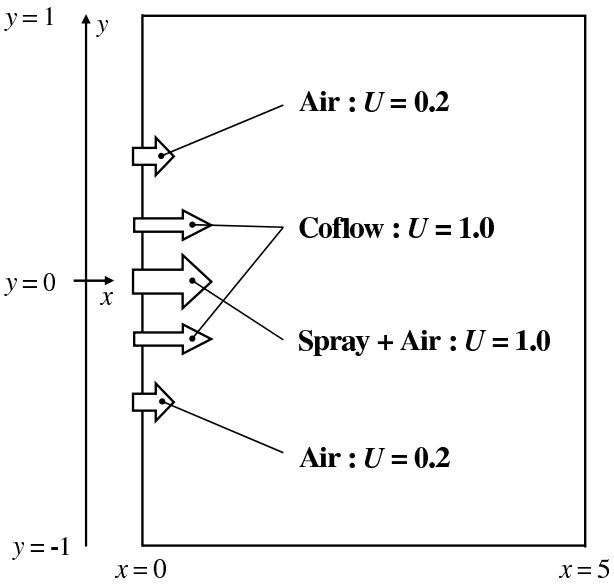
y = 1
y
Air : U = 0.2
Coflow : U = 1.0
y = 0
x
Spray + Air : U = 1.0
Air : U = 0.2
y = -1
x = 0
x = 5

(a)

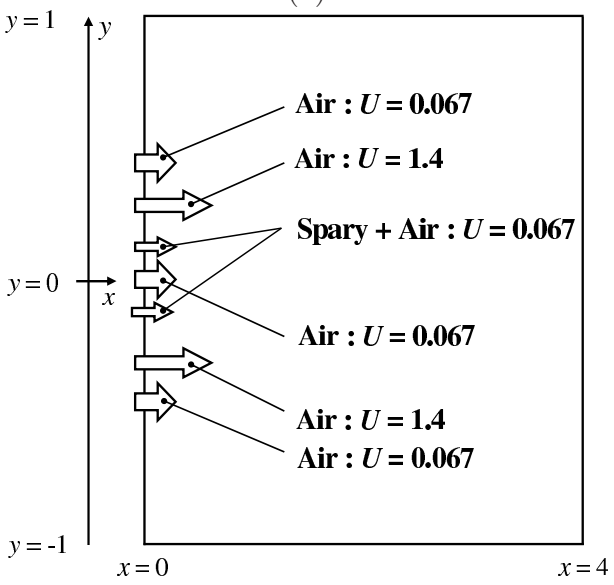
y = 1
y
Air : U = 0.067
Air : U = 1.4
Spary + Air : U = 0.067
y = 0
x
Air : U = 0.067
Air : U = 1.4
Air : U = 0.067
y = -1
x = 0
x = 4

(b)

Figure 1:

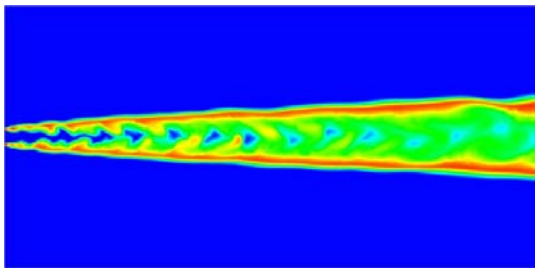

1 8

J-1 (0.1 MPa)

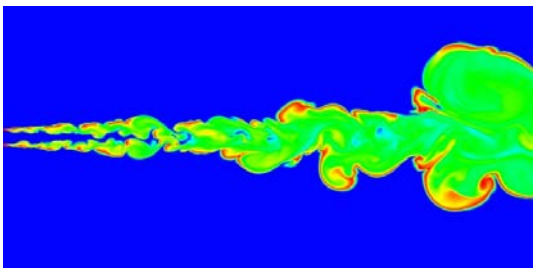

1 8

J-2 (0.5 MPa)

(a)

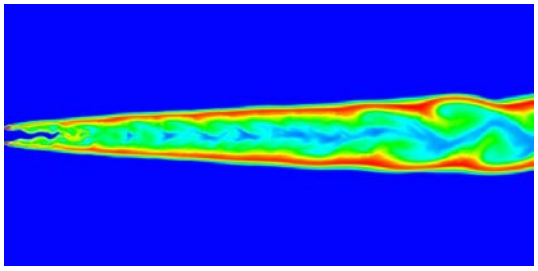

1 8

J-3 (0.1 MPa)

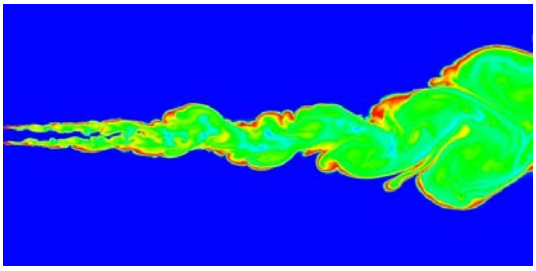

1 8

J-4 (0.5 MPa)

(b)

Figure 2:

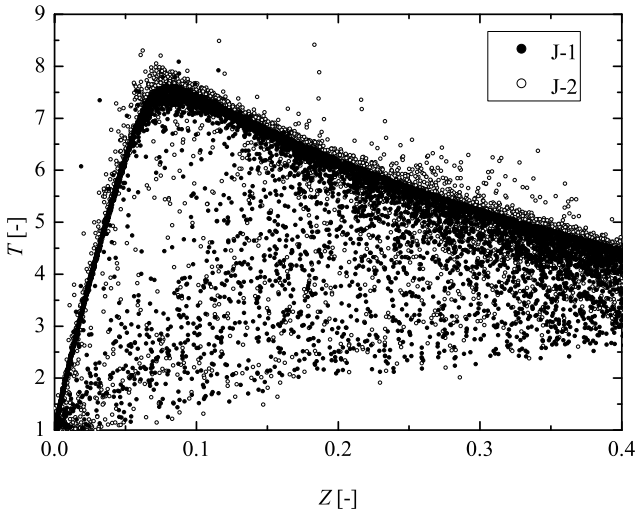

(a)

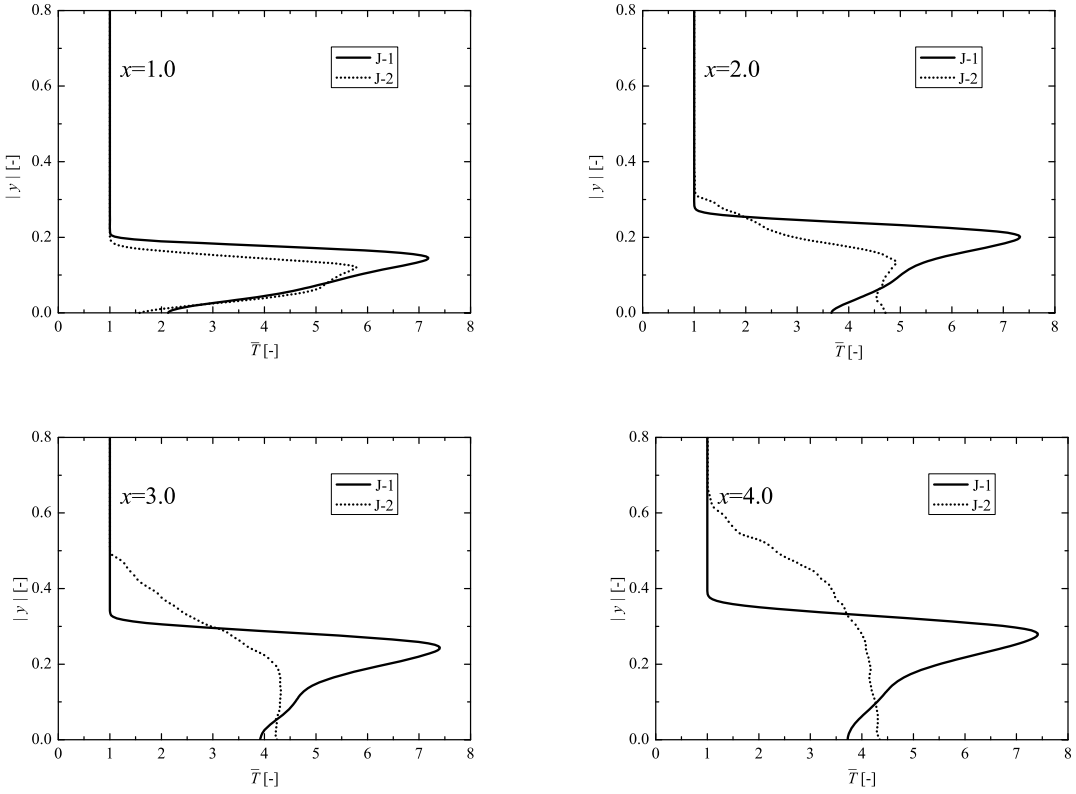

(b)

Figure 3:

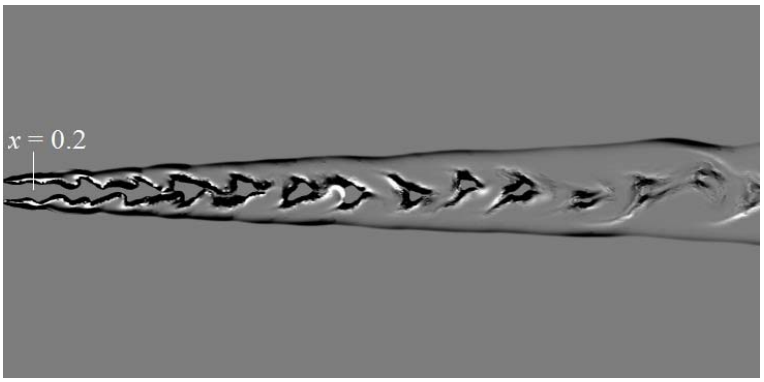

(diffusion)-1 1(premixed)

J-1 (0.1 MPa)

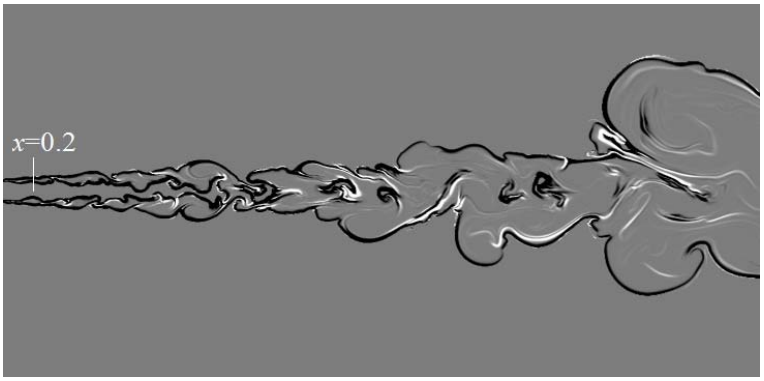

(diffusion)-1 1(premixed)

J-2 (0.5 MPa)

Figure 4:

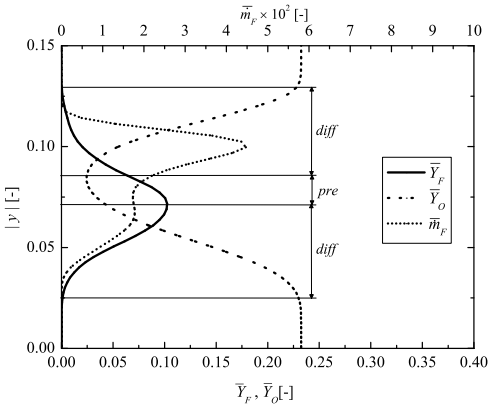

J-1 (0.1 MPa)

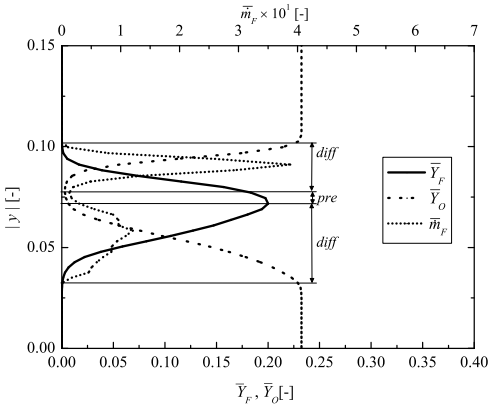

J-2 (0.5 MPa)

Figure 5:

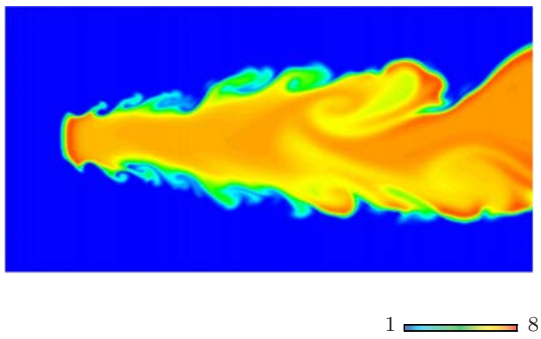

L-1 (0.1 MPa)

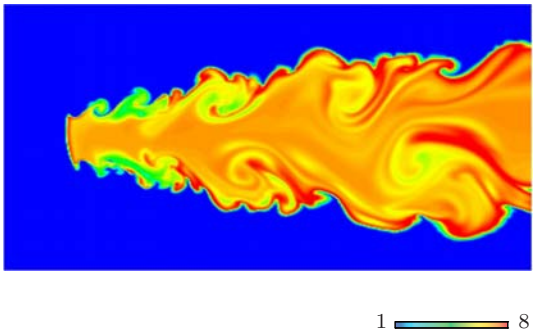

L-2 (0.5 MPa)

(a)

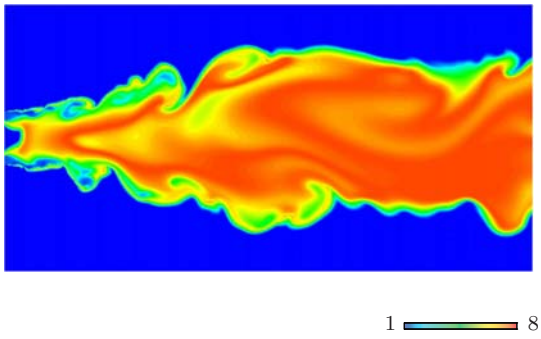

L-3 (0.1 MPa)

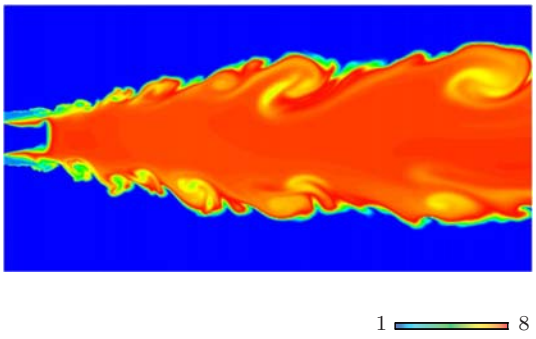

L-4 (0.5 MPa)

(b)

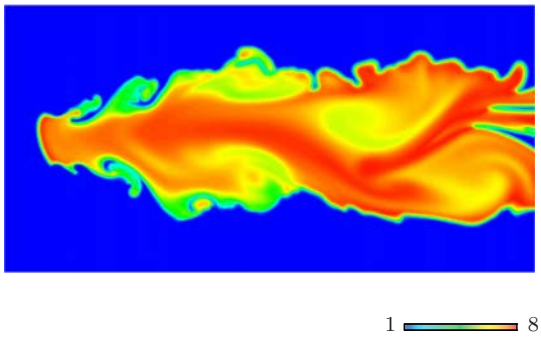

L-5 (0.1 MPa)

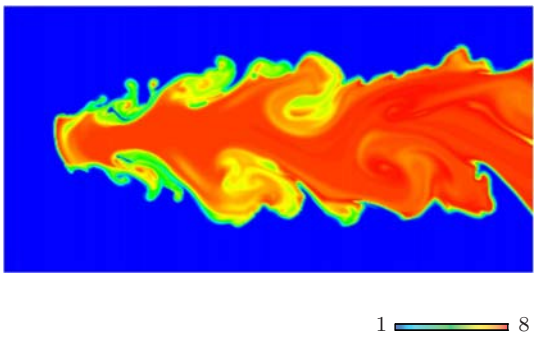

L-6 (0.5 MPa)

(c)

Figure 6:

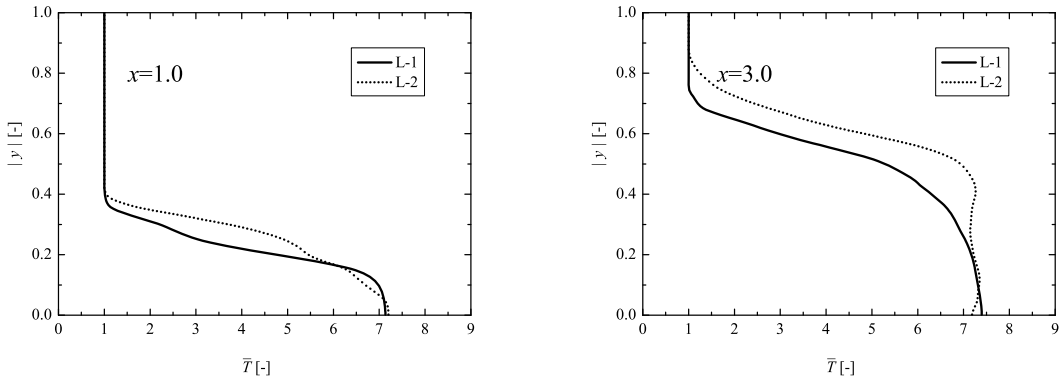

Figure 7:

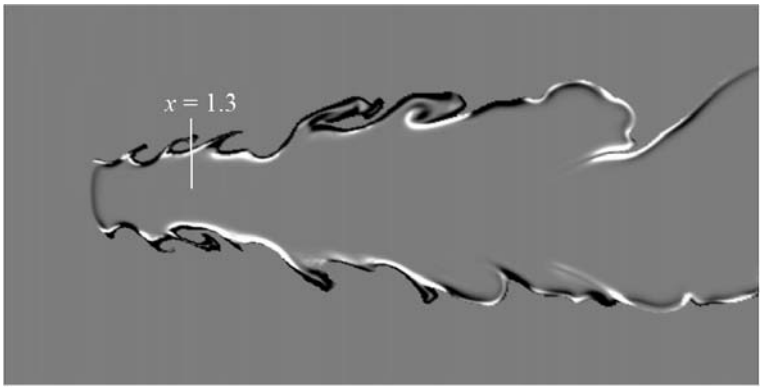

(diffusion)-1 1(premixed)

L-1 (0.1 MPa)

(diffusion)-1 1(premixed)

L-2 (0.5 MPa)

Figure 8:

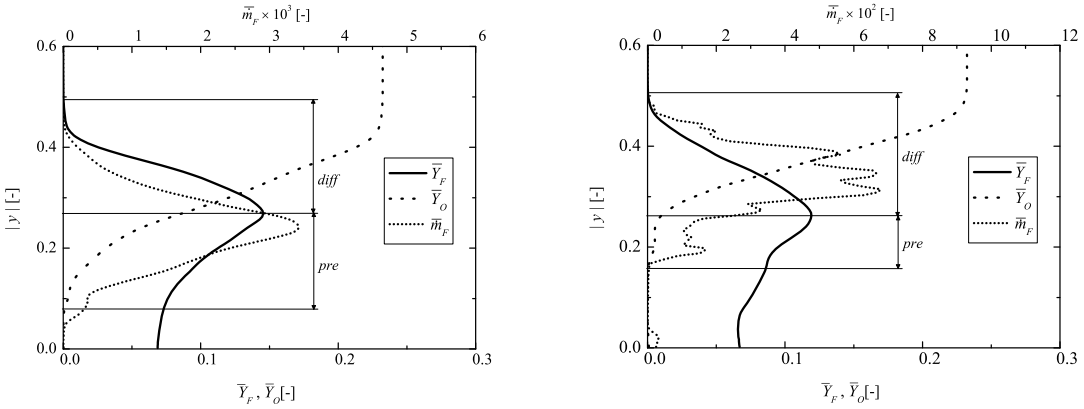

L-1 (0.1 MPa) L-2 (0.5 MPa)

Figure 9:

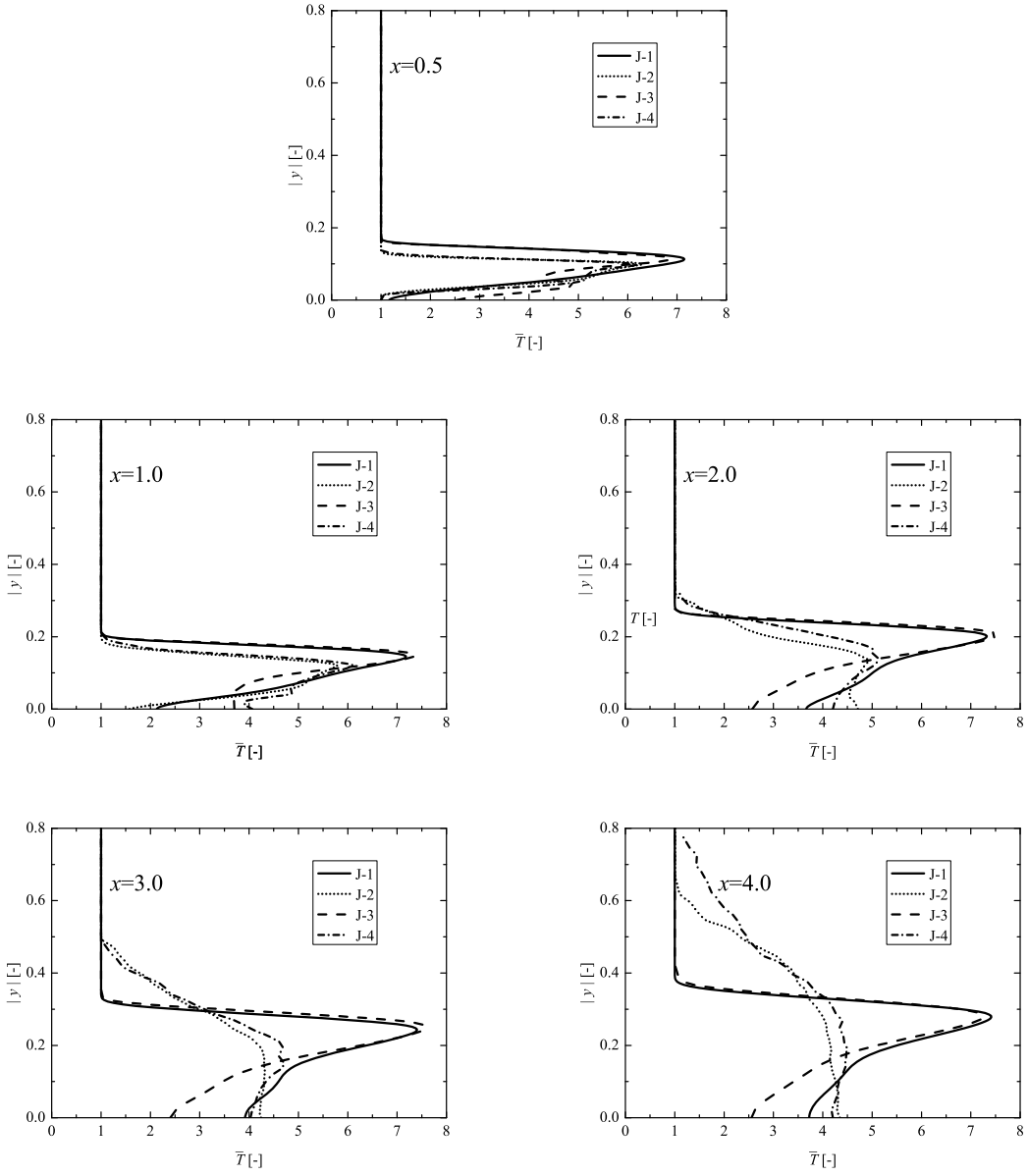

Figure 10:

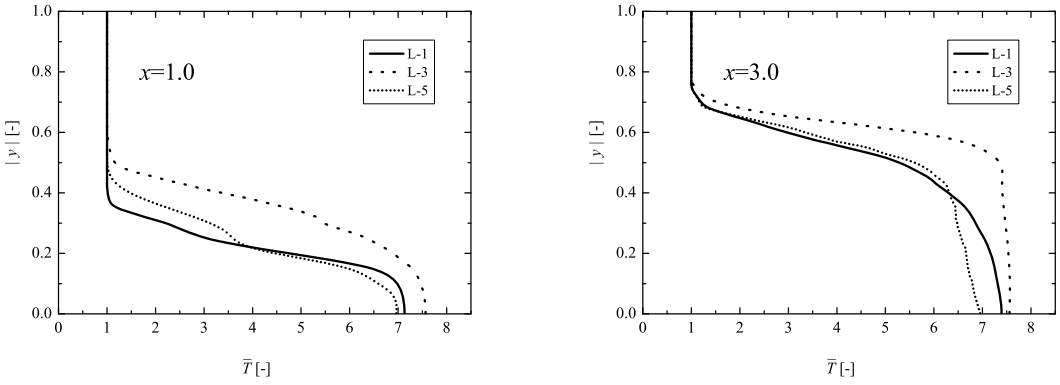

0.1 MPa

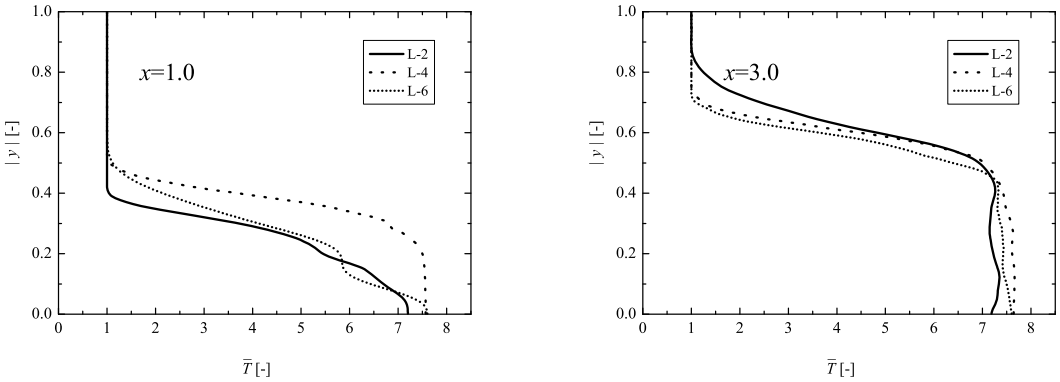

0.5 MPa

Figure 11: